Available online at www.sciencedirect.com

Chemical Engineering Research and Design

journal homepage: www.elsevier.com/locate/cherd

Fluidized bed reforming of methane by chemical looping with cerium oxide oxygen carriers

F. Miccio[a,*], E. Landi[a], A. Natali Murri[a], M. Minelli[b], F. Doghieri[b], A. Storione[b]

[a] Institute of Science, Technology and Sustainability for Ceramics (ISSMC), National Research Council of Italy (CNR), via Granarolo, 64, 48018 Faenza, RA, Italy

[b] Department of Civil, Chemical, Environmental and Materials Engineering (DICAM), Alma Mater Studiorum, University of Bologna, via Terracini 28, 40131 Bologna, Italy

ARTICLE INFO

Article history:
Received 27 November 2022
Received in revised form 29 January 2023
Accepted 4 February 2023
Available online 8 February 2023

Keywords:
CH_4 reforming
Oxygen carrier
Cerium oxide
Fluidized bed

ABSTRACT

Methane reforming is an industrial process for hydrogen production having a high CO_2 footprint that can be mitigated either by using renewable methane, or by recycling carbon dioxide from capture. Methane reforming assisted by an oxygen carrier was currently investigated, being an attractive option for production of hydrogen and carbon monoxide mixtures. The distinctive aspect of present research was the development of three different granular materials based on CeO_2 to be used in fluidized beds, obtained by pelletization and calcination at 900 and 1200 °C of CeO_2 or CeO_2/Al_2O_3 powder. Fluidization and abrasion tests were performed at cold and hot conditions, showing the best attrition resistance of materials calcined at the highest temperature, with attrition rate equal to 0.3 %/h. Conversely, thermogravimetric tests at 900 °C revealed the best performance of CeO_2 granules sintered at lower temperature with respect to the others in terms of oxygen supply capacity, achieving 0.55 of conversion degree. Reforming and regeneration cycles were performed in fluidized bed at 940 °C with CeO_2/Al_2O_3 granules, providing instantaneous methane conversion up to 37 %, high carrier conversion (0.87) and low carbon deposition (2.9 mg/g) during the reforming step.

1. Introduction

Global industrial CO_2 emissions account for more than 30 % of the total emission in the atmosphere (Vogl et al., 2018). Therefore, future use of fossil fuels, also including natural gas, will require the combined carbon capture and storage, having a large impact on the process economics and social acceptance (Rubin et al., 2012). Conversely, hydrogen is a zero-emission and fully sustainable fuel for engines, boilers and furnaces, but it is also a key chemical reactant for several processes in the industry, e.g., hydrogenation, methanol synthesis, ammonia production, etc. (Rambhujun et al., 2020). Furthermore, hydrogen is a possible alternative to coal/coke for steel industries upon production of green hydrogen as reducing agent of iron ores (Pareek et al., 2020).

Methane reforming to syngas is currently the major route for hydrogen production from natural gas (Martino et al., 2021). In this concern, the utilization of biogas obtained by anaerobic digestion or biomass gasification would significantly decrease the carbon footprint. Furthermore, dry reforming of methane (DRM) offers the possibility to valorize carbon dioxide coming from capture/separation, avoiding its storage (Lavoie, 2014). Depending on the methane origin, energy source and adopted process, also including the

* Corresponding author.
E-mail address: francesco.miccio@cnr.it (F. Miccio).

https://doi.org/10.1016/j.cherd.2023.02.007

capture of produced CO_2, the hydrogen may be labeled with different colors (Ajanovic et al., 2022). In particular, "green H_2" refers to a production cycle where all renewable resources are used, e.g., water splitting by photovoltaic electricity; "blue H_2" and "grey H_2" are mainly obtained by natural gas reforming with or without carbon capture, respectively. Thus, methane reforming falls into green or blue H_2 generation, depending on the combination of used resources (renewable or fossil).

Main chemical reactions (R1)–(R3) of the process are reported below, along with standard enthalpies.

$$CH_4 + CO_2 \rightarrow 2H_2 + 2\,CO \qquad \Delta H° = 247.0\ kJ/mol \qquad (R1)$$

$$CH_4 \rightarrow 2H_2 + C \qquad \Delta H° = 74.6\ kJ/mol \qquad (R2)$$

$$2CO \leftrightarrow CO_2 + C \qquad \Delta H° = -172.4\ kJ/mol \qquad (R3)$$

Dry methane reforming DRM (R1) is strongly endothermic and irreversible at T = 1273 K.

The endothermic nature of dry reforming reaction imposes high operating temperature which in turn implies a high energy supply. A common strategy to run the process in less sever condition relies on the utilization of carrier materials, typically metal oxides or mixed oxides with defective structures able to work as source of oxygen or carbon dioxide and as potential catalyst as well (De Vos et al., 2020). However carbon formation appears to compete with the DRM both at high and low temperature due to the side reactions of methane decomposition (R2) and Boudouard reaction (R3), leading to carbon deposition over the catalysts surface and deactivation (Guerrero-Caballero et al., 2019).

Another important reaction is the partial oxidation of methane (R4). This reaction, if carried out by means of a solid oxygen carrier (Adanez et al., 2012) in alternative to pure oxygen from air distillation, would be very attractive from point of view of process intensification and economics, in particular when the carrier also acts as catalyst toward DRM.

$$CH_4 + \tfrac{1}{2}\,O_2 \rightarrow 2H_2 + CO \qquad \Delta H° = -35.9\ kJ/mol \qquad (R4)$$

In this concern, chemical looping partial oxidation and dry reforming of methane can be considered as a possible option for hydrogen production. The process is heterogeneous and the reactants (CH_4 and oxygen carrier) can be kept in contact at high temperature in a suitable reactor (e.g., fluidized bed) with moderate heat exchange.

Cerium belongs to the light rare earth group of the periodic table of elements, being the 25th most abundant element of the common elements in the Earth's crust (Gad, 2014). Besides other applications, cerium oxide or ceria (CeO2) is used for preparation of functionalized ceramic devices (Novik et al., 2015). CeO_2 decomposes via reaction (R5) at high temperature (over 1500 °C), with a stoichiometric loss of oxygen equal to 4.65 wt%. However, the presence of a reducing agent, e.g., CH_4, is very effective for depleting the lattice oxygen at lower temperature. Previous thermodynamic investigation (Storione et al., 2021) pointed out the possibility of using cerium oxide to achieve a complete methane conversion with limited carbon deposition at temperature of around 1173 K. Further, ceria was found to be selective in syngas production even when CO_2 was added to the reforming reactor (Storione et al., 2021). This finding can be also exploited for the reuse of carbon dioxide from decarbonization processes, CO_2 being the oxidant species in the same or in a separate reactor. This last configuration, where CO_2 is employed for regeneration, allows enhancing the flexibility of the overall process from a syngas ratio perspective. Indeed, the oxidation of Ce_2O_3 by CO_2 (reaction (R6)) brings to an additional production of carbon monoxide thus better tuning the final products ratio (Sastre et al., 2022).

$$CeO_2 \leftrightarrow \tfrac{1}{2}\,Ce_2O_3 + 1/4O_2 \qquad \Delta H° = 184.2\ kJ/mol \qquad (R5)$$

$$Ce_2O_3 + CO_2 \leftrightarrow 2\,CeO_2 + CO \qquad \Delta H° = -20.4\ kJ/mol \qquad (R6)$$

Also García-García and Metcalfe (2021) explored the potential of CO_2 as activating species in methane reforming, operated in a looping mode. In CO_2 gaseous atmosphere the carrier oxidation was found to be incomplete and no products of methane total combustion were detected in the further reduction step, thus proving the increase in selectivity towards syngas achievable using carbon dioxide to control the oxidation state of the carrier.

Extensive research was devoted to the development of carbon resistant catalysts and the optimization of catalyst regeneration process to tackle the adverse effect of carbon deposition (Bhavsar and Veser, 2014; Theofanidis et al., 2015). In spite of many efforts, carbon deposition remains a primary obstacle to the industrial implementation of DRM. In this framework, air can be used for the regeneration of the oxygen carrier via chemical looping reforming: the depleted lattice oxygen (O–) during CH_4 oxidation in one reactor (reducer) gets replenished from air in the other reactor (oxidizer) (Neal et al., 2015). The absence of direct contact between CH_4 and oxygen-supplying reagent (e.g., air) prevents the need to use pure oxygen from an expensive air separation unit. In this process scheme, fluidized bed reactors are preferred because of the easiness in accomplishing the oxygen carrier circulation between the reducing and oxidizing reactors (Lyngfelt, 2013), as well as their effectiveness in heat transfer (Kunii and Levenspiel, 1991c). Fluidized beds can also accomplish Ca looping for CO_2 capture and release (Duelli et al., 2015), to be made available in the combined scheme with CeO_2 (reactions (R1), (R4)–(R6)).

In this work, the focus is on the development of a suitable oxygen carrier having also catalytic activity toward dry reforming of methane that can be used as granules in fluidized bed. According to previous studies (Storione et al., 2021), CeO_2 was selected for this purpose, alone or in combination with alumina in order to improve mechanical and structural properties. The novel materials were tested first time in a fluidized bed apparatus and the results analyzed in relation with the internal structure, which changes according to the preparation method. Results of experiments of CH_4 partial oxidation and dry reforming, as well as carrier regeneration at laboratory scale, are reported and commented aiming to provide further insights into material development and process optimization.

2. Methods

2.1. *Materials*

Commercial CeO_2 powder (PIKEM UK, purity 99.9 %) was uniaxially pressed at P = 90 MPa obtaining 20 mm diameter pellets with height of around 30 mm. Afterwards, the pellets were crushed and sieved to the desired size fraction of 0.2–0.4 mm. The same procedure was applied to a mixture 70 %/30 % by weight of CeO_2 and Al_2O_3 (Martinswerk KMS96) powders and, for sake of comparison, to Al_2O_3 alone. The

granules were calcined at a heating rate of 120 °C/h up to 900 °C or 1200 °C and 1 h of dwell time. The samples were correspondingly labeled as Ce900, Ce1200, CeAl1200 and Al1200.

For fluidized bed tests the reference material was quartzite sand (0.2–0.4 mm size). A mixed bed was obtained by mixing quartzite and produced granules.

2.2. Laboratory instruments

Samples of about 80 mg were characterized by a thermogravimetric apparatus (STA 449C Jupiter, Netzsch-Gerätebau GmbH, Germany) at programmed temperature up to 900 °C during 5 cycles of alternating oxidizing and reducing atmosphere respectively obtained flowing air (100 ml/min) for 15 min and CH_4/Ar (4 %, 180 ml/min) for 40 min without gas preheating.

The true density of the materials was calculated by Hepicnometry (Micromeritics AccuPyc II 1340). Microstructural analysis was carried out using a field emission electron scanning microscope FE-SEM (ZEISS SIGMA, Carl Zeiss Microscopy GmbH), equipped with a EDS probe (X-Act INCA Energy 300, Oxford Instruments, UK) on Pt-Pd coated samples, mounted on conductive C tape. The qualitative phase composition of the materials was obtained by X-Ray diffractometry (D8 Advance, Bruker, US). A Micromeritics instrumentation (AutoChem II) was used for temperature programmed reduction (TPR) in hydrogen of fresh samples (around 100 mg).

2.3. Fluidized bed apparatus

A laboratory scale fluidized bed was used for methane reforming (Fig. 1). The reactor was composed by a cylindrical quartz glass tube (20 mm ID and 700 mm high), equipped at the bottom side with a ceramic porous dish, acting as gas distributor. The reactor was vertically installed in an electric ceramic furnace (Watlow Ceramic fiber heater 24″), allowing temperature up to 1000 °C. A K type thermocouple (T) was fixed at the external wall of the quartz tube close to the gas distributor to measure the reactor temperature and then to provide the input signal to the PID temperature controller. In a calibration test the difference between internal and external temperature was determined to be 40 ± 2 °C. An air compressor and a gas bottle (CH_4/N_2 8/92 vol%) provided the fluidizing streams to the reactor, which were controlled by a couple of Brooks SLA-5850 electronic devices. The pressure before the air distributor plate (PI) was measured by means of an electronic manometer (mod. AMECAL ST-8890, AML, UK). The exiting gaseous stream was characterized by means of a continuous gas analyzer (mod. GEIT GAS 3160) for O_2, CO, CO_2, CH_4, and H_2, after filtration and cooling at room temperature.

The test procedure required to alternate air and CH_4/N_2 stages, at temperature of 940 °C. In a specific test, pure CO_2 from bottle instead of air was used during the oxidation step.

3. Results and discussion

3.1. Fluidization behavior

The true densities ρ were 7080, 7160 and 5570 kg/m^3 for Ce900, Ce1200 and CeAl1200, respectively (Table 1), congruently to the enhanced densification of the material at 1200 °C and the addition of a lighter component (Al_2O_3) in the formulation of CeAl1200. The tap density ρ_t of the materials (weight to occupied volume of the granules) follows the same trend (Table 1). For comparison, values are reported also for the quartzite sand. The granule circularity Γ was computed from particle frames with ImageJ open-source software, using the following equation:

$$\Gamma = 4\pi \frac{A_p}{P_p^2} \quad (1)$$

The image analysis was performed on fresh materials, by processing at least 20 particles. In turn, the sphericity Ψ was computed on basis of circularity by multiplying Γ by the factor 0.9 for prolate spheroid (Grace and Ebneyamini, 2021).

The sphericity data are reported in Table 1, resulting very similar to each other for all the materials used.

The minimum fluidization velocity U_{mf} of the three granular materials was determined at room temperature in air by measuring the bottom pressure at increasing and decreasing fluidization velocity. U_{mf} values are reported in Table 1 and are congruent with the density changes. All the three materials belong to the class B of the Geldart's classification (Geldart, 1973), i.e. easily fluidizable powder. According to theoretical estimations (Wen and Yu, 1966), U_{mf} is expected

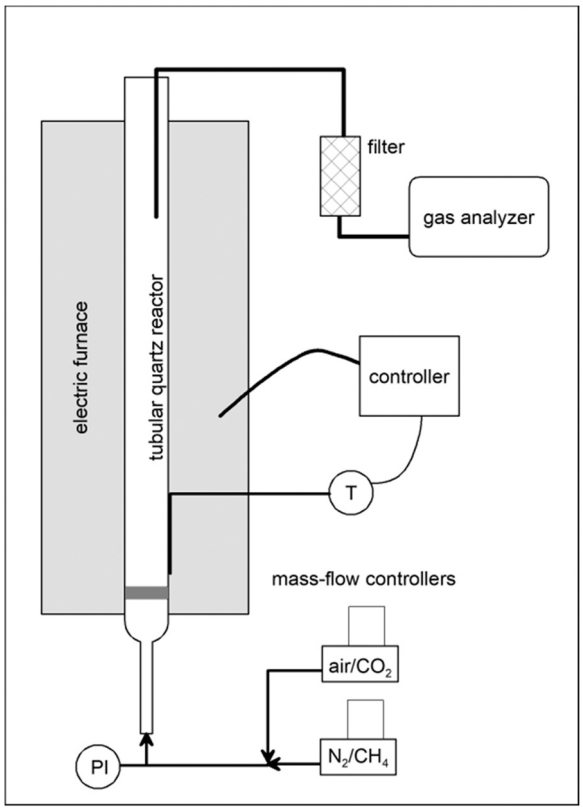

Fig. 1 – Schematic of the FB apparatus.

Table 1 – Properties of materials.

	ρ, kg/m^3	ρ_t, kg/m^3	Ψ, –	U_{mf}, cm/s[a]	E, % h^{-1}
Ce900	7080	2490	0.74	27.2	0.60
Ce1200	7160	2830	0.75	29.8	0.30
CeAl1200	5570	1920	0.74	14.3	0.29/0.50[b]
quartzite	2600	1430	0.73	6.7	–

[a] At 20 °C.
[b] At 850 °C.

to be more than halved from room temperature to 900 °C. The theoretical value of U_{mf} computed via Ergun equation (Kunii and Levenspiel, 1991a) for silica sand at high temperature (900–950 °C) is 2.6 ÷ 2.7 cm/s.

For the mixed bed of quartzite and CeAl1200 some segregation occurred as consequence of the different density and U_{mf}, as proved by fluidization tests carried out in the same reactor at room temperature and scaled fluidization velocity. The quartz sand tended to stay in the upper part of the bed. The bed expansion was around 1.5 times with respect to fixed bed conditions.

The attrition rate E of Ce900, Ce1200 and CeAl1200 was measured in fluidized bed at room temperature, following the procedure adopted by Miccio et al. (2019), by collecting and weighing the elutriated fines Δm_{el} from the fluidized bed in a paper filter Whatman 43 at fixed time interval Δt and fluidization velocity $U = 1.5\ U_{mf}$. The percent elutriation constant E was calculated (Eq. (2)) as the percent ratio between the elutriation rate and the bed inventory (m_{bed})

$$E = 100\frac{\Delta m_{el}}{m_{bed}\,\Delta t} \tag{2}$$

Values of E are reported in Table 1 for the three materials. The higher was the sintering temperature, the lower the attrition rate. Furthermore, the addition of alumina slightly increased the mechanical strength of the granules compared to those formed by CeO_2 alone. The attrition rate resulted similar or somewhat higher compared to other natural or synthetic materials used in thermochemical processes, e.g. olivine (Rapagna et al., 2000), alumina catalyst (Park et al., 2000), and geopolymer composites (Miccio et al., 2017). For CeAl1200 the attrition test was conducted also at hot conditions (T = 850 °C), providing a slightly higher value of E with respect to the corresponding cold test, i.e 0.50 vs. 0.29 % h^{-1}.

3.2. *Thermogravimetric results*

Results of thermogravimetric (TG) tests are displayed in Fig. 2 and summarized in Table 2. The weight change curves (black lines) slightly exceed 100 %, as consequence of a buoyancy effect during temperature increase with consequent change of the gas density.

CeO_2 granules pre-calcined at 900 °C (Ce900) gave rise to the highest weight changes under TG cycling (Table 2). The more compact structure and consequently less reactive surface of the materials calcined at 1200 °C, causing intra-particle diffusion resistance, is a plausible explanation of this finding (see below SEM results).

The oxidation steps, i.e., rising segments, were very fast, a few minutes being enough to get a stable value, while reduction steps would need longer time to achieve stable values and appear incomplete (Fig. 2A–C). For all three samples, the decrease of the minimum values may be related to the increase of performance and reactivity of the material at increasing reduction/oxidation cycle number.

Granules pre-calcined at 1200 °C (Ce1200) interestingly showed a well evident progressive improvement of the weight change ($\Delta W/W_0$) with number of cycles (Fig. 2B), even if the effectiveness in oxygen supply (i.e. weight decrease) was markedly lower if compared to Ce900 granules (Table 2), as consequence of the more compact structure and less available reactive surface characterizing ceramic material when sintered at higher temperature.

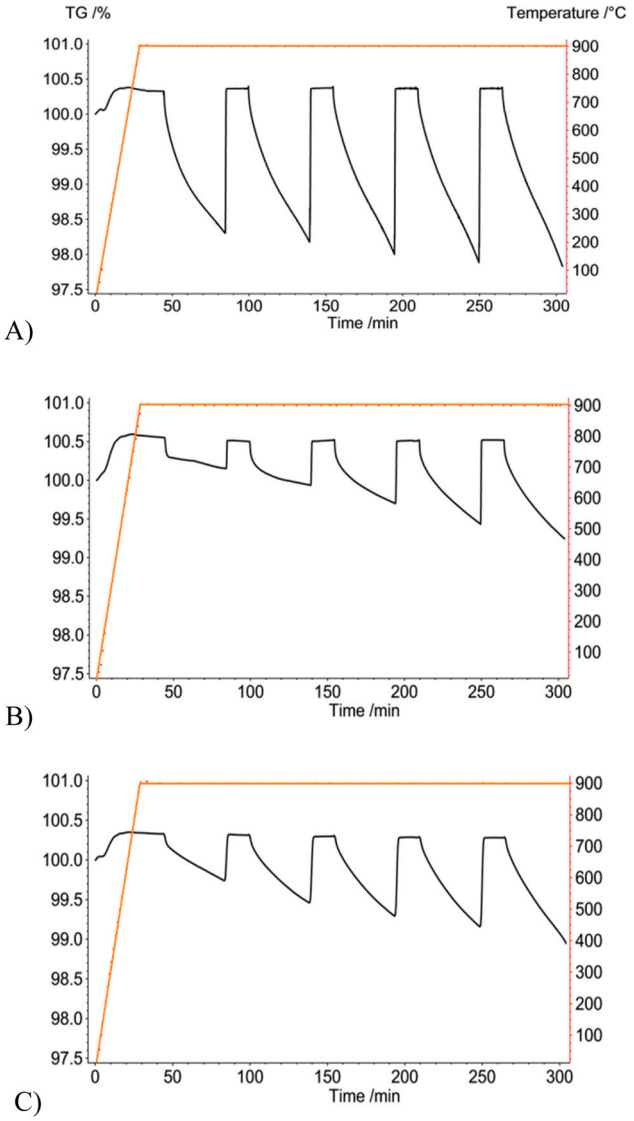

Fig. 2 – Weight changes (black lines) and programmed hoven temperature (red lines) during TG tests. A) Ce900; B) Ce1200; C) CeAl1200.

Table 2 – Results of TG tests. Weight loss, % and tap density.

	$\Delta W/W_0$ 1st cycle	$\Delta W/W_0$ 5th cycle	ρ_t, kg/m^3
Ce900	-2.18	-2.59	2990
Ce1200	-0.96	-1.28	3140
CeAl1200	-0.86 [– 1.23][a]	-1.33 [– 1.90][a]	2350

[a] Values normalized to CeO_2 content.

CeAl1200 granules showed a trend similar to Ce1200 at increasing cycle number, as well as a synergic effect in improving the capability of CeO_2, accounting only for 70 % of the total granule mass, to transfer oxygen. This finding was confirmed by TPR analyses of Ce1200 and CeAl1200 samples that gave H_2 consumption of 3.8 and 2.9 mmol/g, respectively, corresponding to oxygen carrying capability equal to 3.1 and 2.3 wt%. This effect is likely due to the composite microstructure of CeAl1200 pellets allowing higher exposition of active sites to gaseous reactants, as will be discussed later. In fact, the comparison of the values reported in the last column of Table 2 clearly shows that the weight decrease in 5th cycle is similar for Ce1200 and CeAl1200, but it was

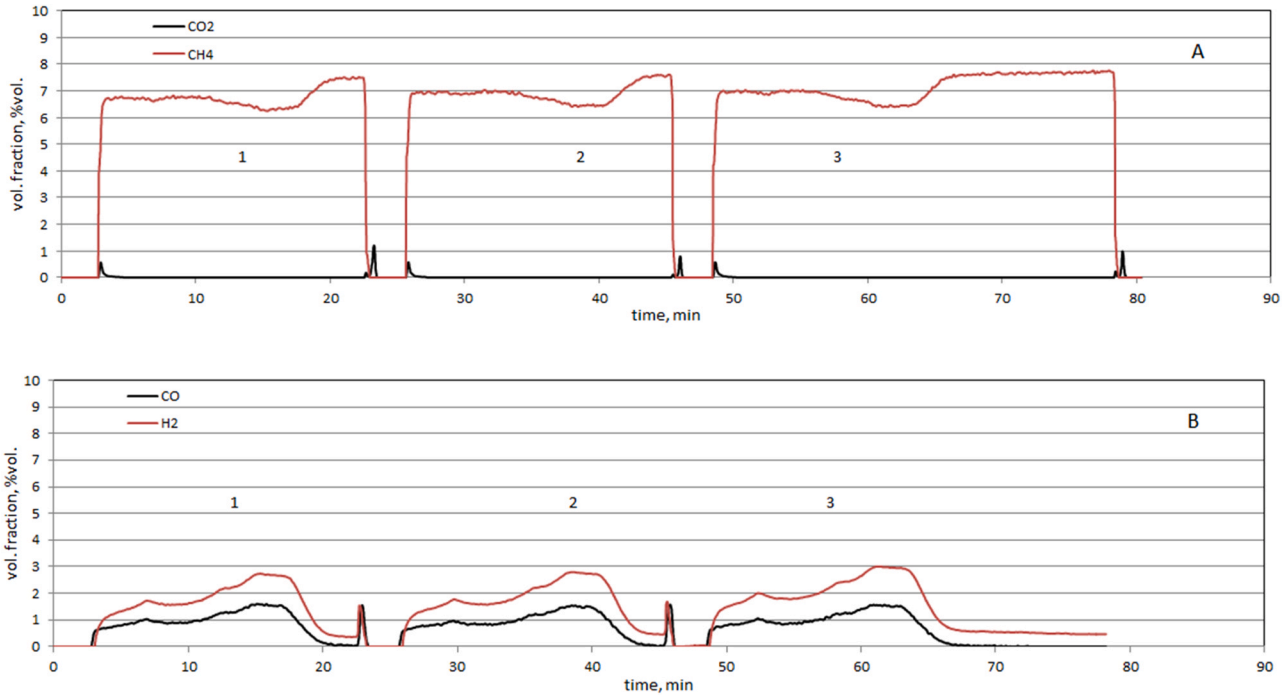

Fig. 3 – Outlet volumetric fraction of CO_2, CH_4 (A) and CO, H_2 (B) in quartzite/CeAl1200 bed at T = 940 °C.

about 50 % larger on the basis of the active compound only, i.e., CeO_2, reported in square brackets. Since the stoichiometric weight losses are 4.7 wt% for Ce900 or Ce1200, and 3.3 wt% for CeAl1200, CeAl1200 exhibited at 5th cycle a higher feature (– 1.90 %) on CeO_2 basis with respect to Ce1200 (– 1.28 %), whilst Ce900 better approached the stoichiometric weight loss (– 2.59 % vs. 4.70 %) with conversion $\xi = 0.55$. It is worth noting that the tap density of the cycled granules (Table 2) increased consistently with the trend observed for the un-cycled materials (Table 1).

3.3. *Fluidized bed results*

Based on results on fluidization behavior and TG tests, CeAl1200 was selected as the granular material for hot fluidization tests, thanks to i) lowest density among three materials, ii) highest mechanical resistance, and iii) suitable high effectiveness in the reforming process. The fluidization velocity was 28.8 cm/s at 940 °C, i.e. two times U_{mf}. The fixed bed height was 20 mm that was roughly doubled under fluidization conditions. This choice was motivated by the need to avoid occurrence of slugs, very likely in small columns, and to limit the attrition of the bed material.

The set-point of the reactor temperature was fixed at 940 °C. According to Storione et al. (2023), the oxidation stage in air was limited to 3 min to prevent excessive oxidation of CeAl1200, since the presence of oxygen vacancies in the lattice are beneficial during reforming (Krenzke and Davidson, 2014). The reducing (reforming) interval was 20 min, corresponding to a slightly longer time than that relating to the methane conversion peak. Furthermore, some tests were prolonged up to full conversion of the oxygen carrier.

Firstly, two FB tests were carried with bed materials of quartzite (10.0 g) and quartzite (10.0 g) plus Al1200 granules (2.0 g), confirming the low reactivity of such materials towards CH_4 reforming. These tests only showed a limited thermal decomposition of methane via reaction (R2) in presence of Al1200, with formation of H_2 and solid carbon, with conversion degree lower than 0.05.

Results of FB tests under alternating cycles in air (3 min) and in reforming atmosphere (20 min) are displayed in Figs. 3 and 4 for a mixed bed of quartzite (5.0 g) and CeAl1200 (5.0 g), at temperature of 940 °C.

Fig. 3 displays the percent volumetric fraction (Y) profiles of CH_4, H_2, CO and CO_2, whilst O_2 is not shown for the sake of figure readability. After the startup, three cycles were repeated with oxidation stage of 3 min and reforming stage of 20 min. A transient response of the system is shown with delayed peaks of H_2 and CO during reforming and a corresponding inverse peak of CH_4.

Carbon formed by CH_4 decomposition was promptly oxidized to CO_2 during the subsequent step of fluidization in air, as demonstrated by the small peaks in Fig. 3A. The last reforming stage from t = 48 min was prolonged until oxygen in CeAl1200 was completely depleted, as denoted by the CO volumetric fraction approaching zero and H_2 achieving a stable value of 0.47 vol%, due to CH_4 thermal decomposition (reaction (R2)).

The repeatability of the oxidation/reforming cycles was well demonstrated by the comparison of the transient profiles in Fig. 4, where the results of 14 consecutive cycles are shown, the last three being carried out with oxidation in pure CO_2 stream. Interestingly, an increase of the hydrogen peak during reforming can be appreciated moving from the first to the fourth cycle, confirming the results of the thermogravimetric tests. The oxidation by CO_2 was effective and the subsequent stages of reforming provided similar response of CO and H_2 concentration.

The measurements of gas concentration were worked out to compute the instantaneous yield X_i of CH_4 to CO and H_2 via Eq. (3), under the hypothesis of nitrogen conservation in the feeding mixture, where i refers either to CO or H_2.

$$X_i = \frac{Y_i}{Y_{CH4,0}} \frac{1 - Y_{CH4,0}}{1 - Y_{CO} - Y_{CO2} - Y_{CH4} - Y_{H2}} \quad (3)$$

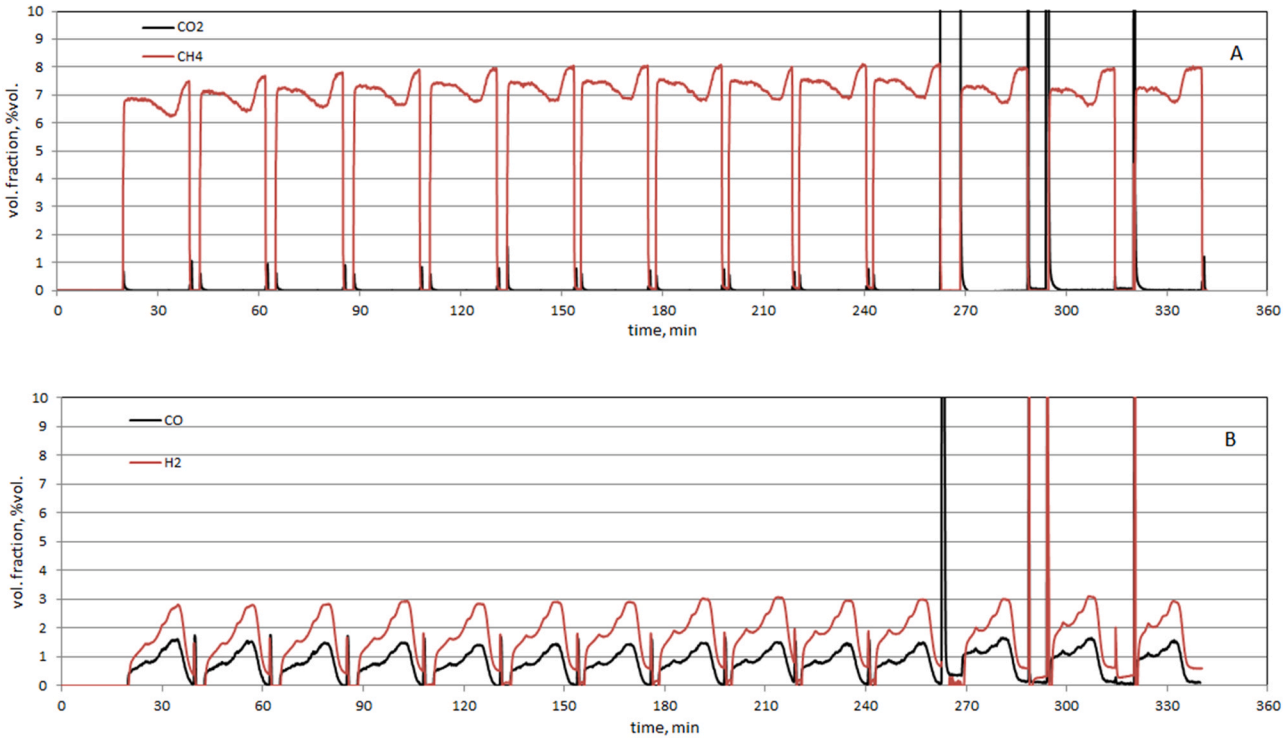

Fig. 4 – Outlet volumetric fraction profiles of CO_2, CH_4 (A) and CO, H_2 (B) in quartzite/CeAl1200 bed at T = 940 °C; last 3 cycles with oxidation in CO_2.

Fig. 5 displays the H_2 instantaneous yield at increasing cycles, where the x axis has been reported as dimensionless periodic time $\theta = \sin(t/\tau)$, τ being the characteristic period of cyclic test conditions. Fig. 5 clearly shows the good repeatability of the results, with good cycle overlapping and without substantial changes of the cycle area. Due to the stoichiometry of reaction (R4) occurring during the reforming stage, the H_2 yield is roughly double than the CO yield, achieving peak values up to 0.37. However, the rather low values of both X_{CO} and X_{H2} with respect to the maximum values (i.e., 1.0 and 2.0, respectively) denote that back-mixing or bubble bypass phenomena occurring in fluidized beds (Kunii and Levenspiel, 1991b) as well as possible particle segregation of the mixed quartzite-CeAl1220 bed (Olivieri et al., 2004) would have determined incomplete contact between gas and solids, slowing down CH_4 conversion. However, these limits in achieving high instantaneous yields may be overcome by adoption of more complex plant configuration, such as multistage fluidized beds, able to reduce back-mixing and bypass phenomena in an heterogeneous process (Schöny et al., 2017; Zhang et al., 2019).

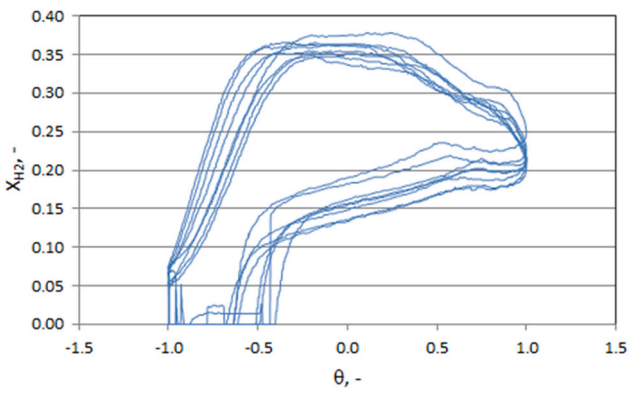

Fig. 5 – Instantaneous CH_4 yield to H_2 and CO in quartzite/CeAl1200 bed at 940 °C.

The percent yield ξ_i for the species i (CO and H_2) during the reforming stage has been computed by numerical integration over the reforming time t_r of the molar fraction Y_i (Eq. (4))

$$\xi_i = 100 \int_{t_0}^{t_r} \frac{Y_i}{Y_{CH4,0}} dt \tag{4}$$

where $Y_{CH4,0}$ is the methane molar fraction in the feed. The results for H_2 and CO are shown in Fig. 6 and the following considerations can be drawn: i) the H_2 yield was always double than CO yield according to the stoichiometry of reaction (R4) (partial oxidation) and the limited reduction time, which hindered the occurrence of reaction (R2) (thermal decomposition); ii) a marked increase of catalyst activity toward n_{H2} can be appreciated during first 5 cycles, in accordance to TG results of Fig. 2, indicating that initial catalyst conditioning improves the process performance; iii) good repeatability of results appears from cycle 6–14 over last ten, even when the catalyst regeneration was carried out by CO_2.

The comparison with the literature data reported by Alvarez-Galvan et al. (2019) for synthetic catalysts based on alumina, rhodium, nickel, some of which also containing ceria, is unfavorable, although the very different reaction conditions must be taken into account, apart from the catalyst composition. They reported CO yield comprised between 40 % and 85 % at T = 750 °C, with reaction time of 60 min and a sample of 100 mg. It must be noted that the loss of performance of CeAl1200 is attributable to the initial evolution of the H_2 and CO during reduction (Fig. 4), with a delay of around 12 min in achieving the peak. The optimization of the carrier, as well as of the operating conditions may result in substantial increase of the yield, i.e. rather double if the peak is promptly reached.

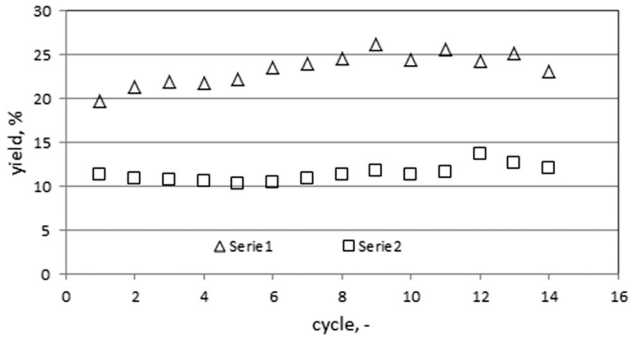

Fig. 6 – CH_4 yields to H_2 and CO in quartzite/CeAl1200 bed at 940 °C.

The conversion CeAl1200 has been evaluated (Eq. (5)) on the basis of n_{CO} (Eq. (4)) assuming that CO was generated by depleting the oxygen atoms initially available in the carrier and CO_2 was negligible. The reduction of one CeO_2 molecule makes available 1/2 atom of oxygen, according to reaction (R5).

$$\xi = 2\frac{n_{CO}}{n_{CeO2}} \tag{5}$$

Eq. (5) neglects the release of oxygen from Al_2O_3 that is thermodynamically possible only at temperature over 1200 °C. The average ξ value over first ten cycles of Fig. 6 is equal to 0.87 ± 0.03. The limited deviation again confirms the good repeatability of the cycles and, more notably, proves the large conversion degree of the CeAl1200 granules in fluidized bed with respect to TG tests, owing to the improved mixing and mass diffusion of FB operation.

Temperature increments up to 30 °C have been recorded during bed regeneration in air via reaction (R5), as consequence of the oxidation of Ce_2O_3 and of the deposited carbon (coke). The latter has been estimated by integration of CO and CO_2 volumetric fraction during carrier regeneration in air. The average value for tests of Fig. 3 was equal to 2.9 mg/g (referred to CeAl1200 weight), confirming the occurrence of little coke deposition over ceria (Teh et al., 2021). Conversely, the temperature increase was limited to less than 10 °C in the case of catalyst regeneration by CO_2 (reaction (R6)), due to the slower carbon oxidation kinetics in CO_2 with respect to O_2 (Laurendeau, 1978).

The samples obtained after FB tests, upon visual inspection and sieving, exhibited particle agglomeration neither between same granules, nor between quartz and CeAl1200. This finding was also confirmed by the SEM analyses (see below).

3.4. *Characterization of samples from experiments*

SEM images reported in Fig. 7 show the effect of the different calcining temperatures on the microstructure of the CeO_2 granules. Confirming what previously anticipated, those treated at higher temperature (Fig. 7b) exhibit a more compact and close-packed microstructure, with a more widespread and accentuated necks formation between the constituting particles that appear clearly enlarged/grown, in turn determining a decrease in the material porosity and in the exposed surface.

Fig. 8 displays the macroscopic and microscopic features of the composite of CeAl1200 granules before and after fluidized bed tests. The operation at high temperature didn't result in macroscopic changes on the tested granules. After cycling in the reactor, composite granules experienced some little shrinkage (Fig. 8a, b), in agreement with the tap density increase found after TG test. No significant breaking phenomena have been detected, apart from some cracks on the surface, confirming the good mechanical stability of the material, nor was any kind of agglomeration noticed between the granules. Compared to un-tested granules, the cycled ones appear to have suffered only a partial loss of surface material, showing a smoother and more compact outer surface. Such finding is in agreement with the abrasion evidenced during reactor tests.

The presence of alumina in the composite material interferes with the sintering degree of the CeO_2 particles, acting as a physical and mechanical hindrance to the formation of densification areas among CeO_2 particles on the surface and within the granule, allowing to maintain a certain degree of interparticle porosity after cycling (Fig. 8c, d). The microstructure features may explain the progressive improvement with number of cycles detected during tests. The formation of a stable porosity network on the surface and inside the granule allows the gas to progressively enter inside the granule and face with still fresh material. Thus, not only lattice oxygen available at the external surface of the granules was available for methane conversion, but also internal sites. It is worth recalling that the granules were prepared starting from micronic powder that was sintered at high temperature, not achieving fusion and allowing to obtain an effective pore network.

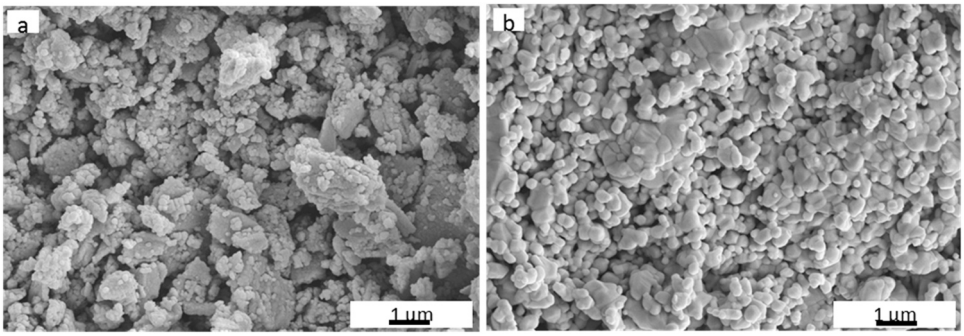

Fig. 7 – Microstructure for Ce900 (a) and Ce1200 (b) before testing.

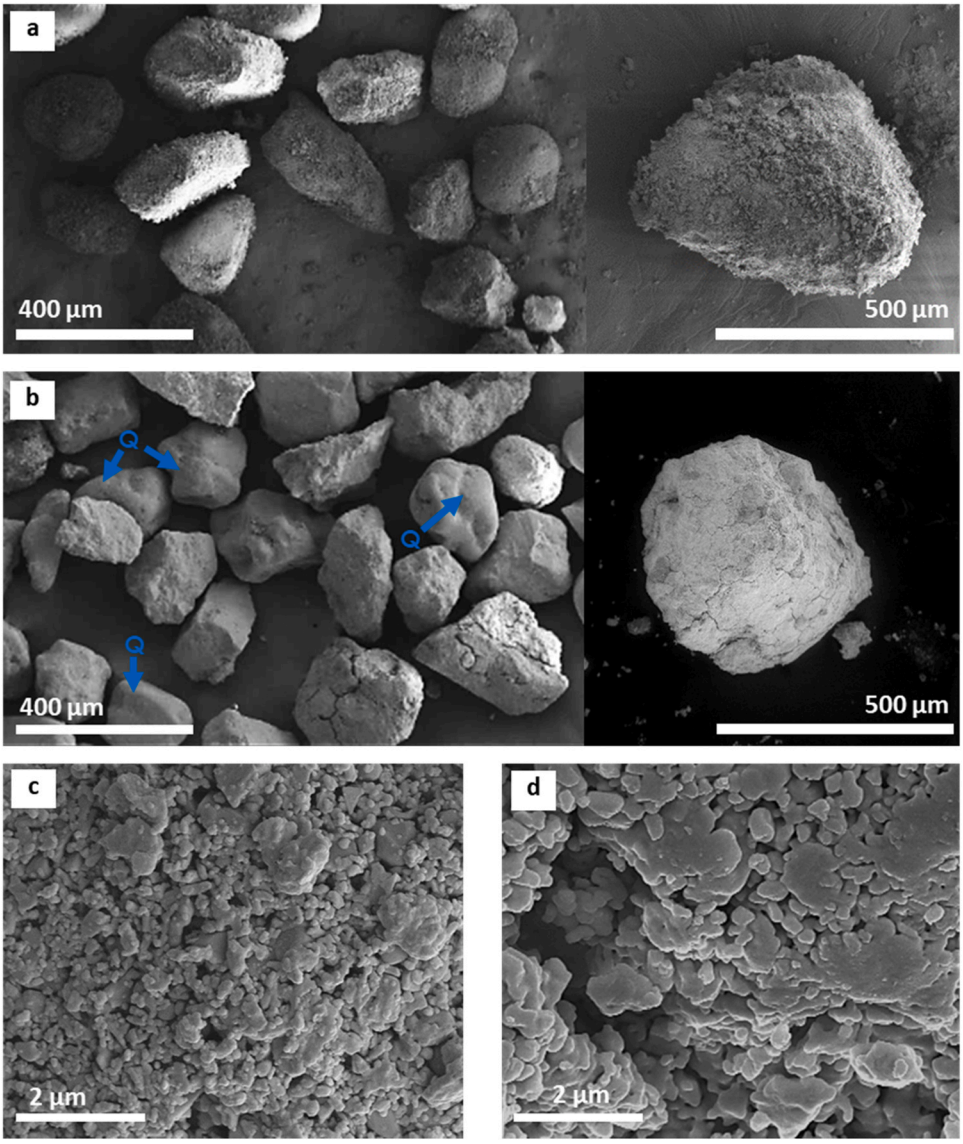

Fig. 8 – CeAl1200 granules before (a, c) and after (b, d) fluidized bed testing (Q: quartzite sand granules).

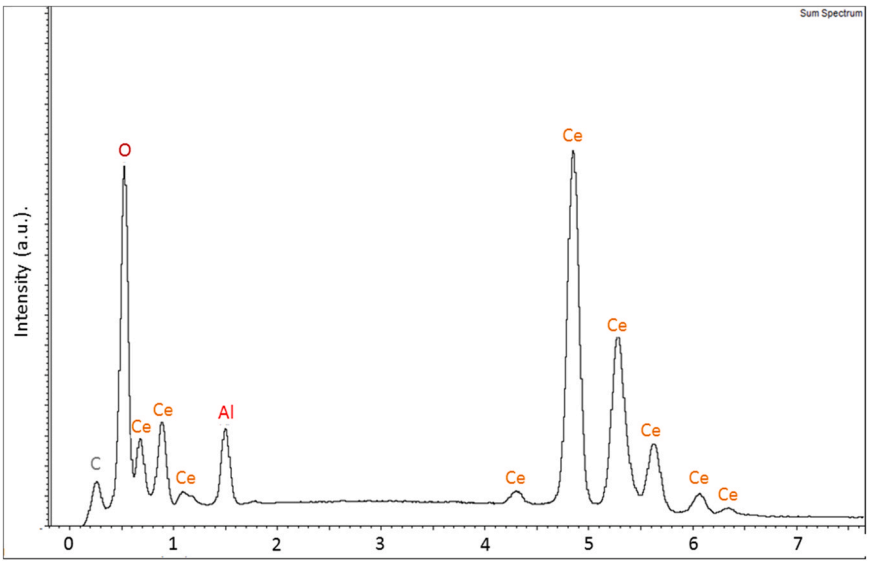

Fig. 9 – EDS spectrum of composite material after reactor testing.

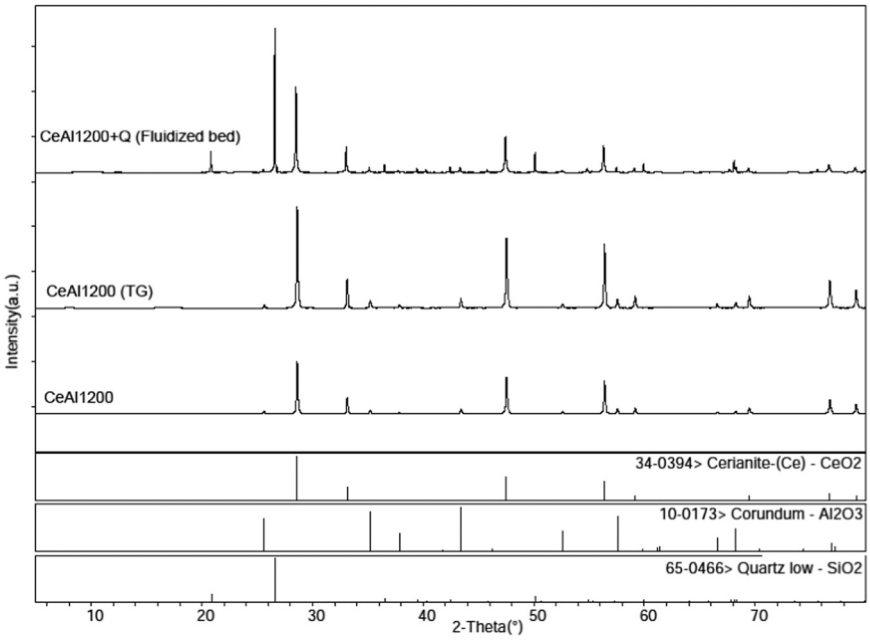

Fig. 10 – XRD patterns for as given CeAl1200, after TG tests and after fluidized bed tests (with quartzite sand).

In addition, no macroscopic agglomeration phenomena have been found among granules of CeAl and quartzite sand in the reactor bed. Further, the EDS spectrum (Fig. 9) detected on several areas of the composite material after reactor testing evidenced the presence of the constituting elements (Ce, Al and O) only, proving no interactions, such as diffusion of Si, occurred with quartzite sand (Semberg et al., 2011).

XRD patterns (Fig. 10) confirm the thermal stability of the composite phases against cycling treatments in fluid bed and in TG at high temperature, since there is no formation of any mixed oxidic phase between Ce and Al, nor between the composite phases and the quartzite added to the reactor. The only phases found in the material, similarly to the non-cycled sample, are cerianite and corundum, providing a further confirmation of the material stability.

4. Conclusions

An experimental research has been carried out with CeO_2 based oxygen carrier in thermo-balance and lab-scale fluidized bed. The results showed that the developed materials are effective towards CH_4 partial oxidation with low carbon deposition, less than 3.0 mg/g. The highest effectiveness, up to 55 % of the theoretical limit, was achieved in TG tests for materials calcined at 900 °C, but higher mechanical resistance (attrition rate of 0.30 vs. 0.60 %/h) was obtained in abrasion tests for those calcined at 1200 °C.

Using a mixture of CeO_2 and Al_2O_3 powders (70/30 wt%) for the production of composite granules resulted in an interesting synergy, since similar weight changes were obtained in TG tests for CeO_2 alone and composite material, thanks to improvements of the internal microstructure of the granule in presence of Al_2O_3.

Optimized cycles of reforming and carrier oxidation tests were carried out at 940 °C in fluidized bed with at least 5 g of granular carrier, providing first and novel insights for the exploitation of this material in a commercial process: instantaneous CH_4 conversion to H_2 and CO achieved a peak of 37 %, CO yield over the reduction step was up to 13 % of the fed methane, and the carrier conversion was very high (87 %). The cycles showed a good repeatability of results, proving the stability of the material in near real conditions, confirmed by SEM and XRD analyses of the obtained samples, showing limited changes of microstructure and phases.

The oxidation of the depleted oxygen carrier by means of CO_2 was successfully carried out, opening the possibility of carbon dioxide use in such process.

Improvements of oxygen release kinetics, with respect to the granule microstructure, as well as the investigation of fluidization operating conditions and scalability, taking into account the evaluation of dimensionless parameters that correlate chemical reaction and diffusional transport in the pellets, the limits of heat/mass transfer, the segregation phenomena, the possible hotpot formation and others practical aspects, are valuable issues for further development of the research.

Declaration of Competing Interest

The authors declare that they have no known competing financial interests or personal relationships that could have appeared to influence the work reported in this paper.

Acknowledgements

The research has been funded by the Italian National Programme "Ricerca e Sviluppo di Tecnologie per la Filiera dell'Idrogeno - AdP Italian Ministery MiTE - ENEA, Mission 2, Comp. 2.3.5, PNRR, 2022-2025".

References

Adanez, J., Abad, A., Garcia-Labiano, F., Gayan, P., de Diego, L.F., 2012. Progress in chemical-looping combustion and reforming technologies. Prog. Energy Combust. Sci. 38, 215–282.

Ajanovic, A., Sayer, M., Haas, R., 2022. The economics and the environmental benignity of different colors of hydrogen. Int. J. Hydrog. Energy.

Alvarez-Galvan, C., Melian, M., Ruiz-Matas, L., Eslava, J.L., Navarro, R. M., Ahmadi, M., Roldan Cuenya, B., Fierro, J.L.G., 2019. Partial oxidation of methane to syngas over nickel-based catalysts: influence

of support type, addition of rhodium, and preparation method. Front. Chem., 7.
Bhavsar, S., Veser, G., 2014. Chemical looping beyond combustion: production of synthesis gas via chemical looping partial oxidation of methane. RSC Adv. 4, 47254–47267.
De Vos, Y., Jacobs, M., Van Der Voort, P., Van Driessche, I., Snijkers, F., Verberckmoes, A., 2020. Development of stable oxygen carrier materials for chemical looping processes—a review. Catalysts 10.
Duelli, G., Charitos, A., Diego, M.E., Stavroulakis, E., Dieter, H., Scheffknecht, G., 2015. Investigations at a 10kWth calcium looping dual fluidized bed facility: limestone calcination and CO_2 capture under high CO_2 and water vapor atmosphere. Int. J. Greenh. Gas Control 33, 103–112.
Gad, S.C., 2014. Cerium. In: Wexler, P. (Ed.), Encyclopedia of Toxicology, Third edition. Academic Press, Oxford, pp. 773–775.
García-García, F.R., Metcalfe, I.S., 2021. Chemical looping dry reforming of methane using mixed oxides of iron and cerium: operation window. Catal. Commun. 160, 106356.
Geldart, D., 1973. Types of gas fluidization. Powder Technol. 7, 285–292.
Grace, J.R., Ebneyamini, A., 2021. Connecting particle sphericity and circularity. Particuology 54, 1–4.
Guerrero-Caballero, J., Kane, T., Haidar, N., Jalowiecki-Duhamel, L., Löfberg, A., 2019. Ni, Co, Fe supported on Ceria and Zr doped Ceria as oxygen carriers for chemical looping dry reforming of methane. Catal. Today 333, 251–258.
Krenzke, P.T., Davidson, J.H., 2014. Thermodynamic analysis of syngas production via the solar thermochemical cerium oxide redox cycle with methane-driven reduction. Energy Fuels 28, 4088–4095.
Kunii, D., Levenspiel, O., 1991a. Chapter 3 – fluidization and mapping of regimes. In: Kunii, D., Levenspiel, O. (Eds.), Fluidization Engineering, Second edition. Butterworth-Heinemann, Boston, pp. 61–94.
Kunii, D., Levenspiel, O., 1991b. Chapter 5 – bubbles in dense beds. In: Kunii, D., Levenspiel, O. (Eds.), Fluidization Engineering, Second edition. Butterworth-Heinemann, Boston, pp. 115–135.
Kunii, D., Levenspiel, O., 1991c. Chapter 13 – heat transfer between fluidized beds and surfaces. In: Kunii, D., Levenspiel, O. (Eds.), Fluidization Engineering, Second edition. Butterworth-Heinemann, Boston, pp. 313–336.
Laurendeau, N.M., 1978. Heterogeneous kinetics of coal char gasification and combustion. Prog. Energy Combust. Sci. 4, 221–270.
Lavoie, J.-M., 2014. Review on dry reforming of methane, a potentially more environmentally-friendly approach to the increasing natural gas exploitation. Front. Chem. 2.
Lyngfelt, A., 2013. 20 – chemical looping combustion (CLC). In: Scala, F. (Ed.), Fluidized Bed Technologies for Near-Zero Emission Combustion and Gasification. Woodhead Publishing, pp. 895–930.
Martino, M., Ruocco, C., Meloni, E., Pullumbi, P., Palma, V., 2021. Main hydrogen production processes: an overview. Catalysts 11.
Miccio, F., Murri, A.N., Medri, V., Landi, E., 2019. Utilization of fireclay for preventing fluidized-bed agglomeration during biomass thermochemical processing. Ind. Eng. Chem. Res. 58, 23498–23507.
Miccio, F., Natali Murri, A., Landi, E., 2017. Synthesis and characterization of geopolymer oxygen carriers for chemical looping combustion. Appl. Energy 194, 136–147.
Neal, L., Shafiefarhood, A., Li, F., 2015. Effect of core and shell compositions on MeO_x@$La_ySr_{1-y}FeO_3$ core–shell redox catalysts for chemical looping reforming of methane. Appl. Energy 157, 391–398.
Novik, N.N., KonakovIvan, V.G., Archakov, I.Y., 2015. Zirconia and ceria based ceramics and nanoceramics – a review on electrochemical and mechanical properties. Rev. Adv. Mater. Sci. 40, 188–207.
Olivieri, G., Marzocchella, A., Salatino, P., 2004. Segregation of fluidized binary mixtures of granular solids. AIChE J. 50, 3095–3106.
Pareek, A., Dom, R., Gupta, J., Chandran, J., Adepu, V., Borse, P.H., 2020. Insights into renewable hydrogen energy: recent advances and prospects. Mater. Sci. Energy Technol. 3, 319–327.
Park, Y.S., Kim, H.S., Shun, D., Song, K.S., Kang, S.K., 2000. Attrition characteristics of alumina catalyst for fluidized bed incinerator. Korean J. Chem. Eng. 17, 284–287.
Rambhujun, N., Salman, M.S., Wang, T., Pratthana, C., Sapkota, P., Costalin, M., Lai, Q., Aguey-Zinsou, K.-F., 2020. Renewable hydrogen for the chemical industry. MRS Energy Sustain., 7, 33.
Rapagna, S., Jand, N., Courson, C., Petit, C., Kiennemann, A., Foscolo, P. U., 2000. Nickel based catalysts in the steam gasification of biomass. In: Proceedings of the World Conference and Exhibition on Biomass for Energy and Industry. Sevilla, Spain, pp. 1646–9.
Rubin, E.S., Mantripragada, H., Marks, A., Versteeg, P., Kitchin, J., 2012. The outlook for improved carbon capture technology. Prog. Energy Combust. Sci. 38, 630–671.
Sastre, D., Galván, C.Á., Pizarro, P., Coronado, J.M., 2022. Enhanced performance of CH_4 dry reforming over $La_{0.9}Sr_{0.1}FeO_3$/YSZ under chemical looping conditions. Fuel 309 (122122).
Schöny, G., Dietrich, F., Fuchs, J., Pröll, T., Hofbauer, H., 2017. A multistage fluidized bed system for continuous CO_2 capture by means of temperature swing adsorption – first results from bench scale experiments. Powder Technol. 316, 519–527.
Semberg, P., Rutqvist, A., Andersson, C., Bjorkman, B., 2011. Interactions between iron oxides and the additives quartzite, calcite and olivine in magnetite based pellets. ISIJ Int. 51, 173–180.
Storione, A., Boscherini, M., Miccio, F., Landi, E., Minelli, M., Doghieri, F., 2023. Investigation on optimal process times for methane looping reforming with CeO_2 as oxygen carrier. Chem. Eng. J (submitted for publication).
Storione, A., Minelli, M., Doghieri, F., Landi, E., Miccio, F., 2021. Thermodynamic study on the feasibility of a new combined chemical looping process for syngas production. Chem. Eng. Trans. 86, 1267–1272.
Teh, L.P., Setiabudi, H.D., Timmiati, S.N., Aziz, M.A.A., Annuar, N.H.R., Ruslan, N.N., 2021. Recent progress in ceria-based catalysts for the dry reforming of methane: a review. Chem. Eng. Sci. 242, 116606.
Theofanidis, S.A., Galvita, V.V., Poelman, H., Marin, G.B., 2015. Enhanced carbon-resistant dry reforming Fe-Ni catalyst: role of Fe. ACS Catal. 5, 3028–3039.
Vogl, V., Åhman, M., Nilsson, L.J., 2018. Assessment of hydrogen direct reduction for fossil-free steelmaking. J. Clean. Prod. 203, 736–745.
Wen, C.Y., Yu, Y.H., 1966. A generalized method for predicting the minimum fluidization velocity. AIChE J. 12, 610–612.
Zhang, C., Qian, W., Wang, Y., Luo, G., Wei, F., 2019. Heterogeneous catalysis in multi-stage fluidized bed reactors: from fundamental study to industrial application. Can. J. Chem. Eng. 97, 636–644.